THE ROYAL SOCIETY

Linear elastic contact of the Weierstrass profile†

BY M. CIAVARELLA[1]‡, G. DEMELIO[2], J. R. BARBER[3] AND YONG HOON JANG[3]

[1]*Department of Mechanical Engineering, University of Southampton, Highfield, Southampton SO17 1BJ, UK*

[2]*Dipartimento di Progettazione e Produzione Industriale, Politecnico di Bari, Viale Japigia 182, 70126 Bari, Italy*

[3]*Department of Mechanical Engineering and Applied Mechanics, University of Michigan, Ann Arbor, MI 48109-2125, USA*

Received 12 January 1999; revised 18 May 1999; accepted 2 June 1999

A contact problem is considered in which an elastic half-plane is pressed against a rigid fractally rough surface, whose profile is defined by a Weierstrass series. It is shown that no applied mean pressure is sufficiently large to ensure full contact and indeed there are not even any contact areas of finite dimension—the contact area consists of a set of fractal character for all values of the geometric and loading parameters.

A solution for the partial contact of a sinusoidal surface is used to develop a relation between the contact pressure distribution at scale $n-1$ and that at scale n. Recursive numerical integration of this relation yields the contact area as a function of scale. An analytical solution to the same problem appropriate at large n is constructed following a technique due to Archard. This is found to give a very good approximation to the numerical results even at small n, except for cases where the dimensionless applied load is large.

The contact area is found to decrease continuously with n, tending to a power-law behaviour at large n which corresponds to a limiting fractal dimension of $(2-D)$, where D is the fractal dimension of the surface profile. However, it is not a 'simple' fractal, in the sense that it deviates from the power-law form at low n, at which there is also a dependence on the applied load. Contact segment lengths become smaller at small scales, but an appropriately normalized size distribution tends to a limiting function at large n.

Keywords: multifractals; Weierstrass; contact mechanics; rough surfaces; asperities; multiscale models

1. Introduction

Real surfaces are rough on the microscopic scale and the effect of roughness on the contact process, particularly in sliding contact, forms the basis of most models of friction and wear. Contact is generally expected to be restricted to the highest

† The authors dedicate this paper to the memory of Dr J. F. Archard, 1918–1989.

‡ Present address: CNR-IRIS Computational Mechanics of Solids, str. Crocefisso, 2/B, 70126 Bari, Italy.

points of the surface and hence early models of contact introduced the concept of a distribution of 'asperities' or peaks, whose contact behaviour mimics that of the real surface. An important breakthrough in this field was made by Greenwood & Williamson (1966), who showed that if identical asperities were distributed according to an exponential distribution, the relations between macroscopic quantities such as total normal and tangential load, total actual contact area and thermal contact conductance would all be linear. With a more realistic Gaussian height distribution, these relations cease to be strictly linear, but the ratio between normal and tangential force in sliding varies sufficiently slowly with load to provide what is still one of the more convincing explanations of Amonton's law of friction.

Greenwood & Williamson's (1966) results focused attention on the importance of the asperity height distribution and many subsequent advances have been made in characterizing surfaces using random process theory (Nayak 1971; Whitehouse & Phillips 1978, 1982; Greenwood 1984). At the same time, improvements in experimental methods have increased the bandwidth of surface profile measurements and revealed the existence of a hierarchy of scales up to the limits of experimental discrimination (Mandelbrot 1982; Russ 1994; Lopez *et al.* 1994; Majumdar & Bhushan 1995). This is an embarrassment to asperity model theories, because the definition of an asperity is scale dependent. Thus, whereas with a coarse measuring system (or a large sampling interval) we see only a few asperities of large radius of curvature, as the experimental system is refined, we see more and more asperities of ever decreasing radius. In a remarkably prescient paper, Archard (1957) proposed just such a model to explain some of the characteristics of the elastic contact of two rough surfaces.

Typical surface profiles exhibit a power-law spectral density $P(\omega) = C\omega^{-q}$ at high frequencies ω, suggesting that a fractal description of the surface and the contact process would be more appropriate (Lopez *et al.* 1994; Majumdar & Bhushan 1990, 1995; Borodich & Mosolov 1992; Borodich & Onishchenko 1999; Borri-Brunetto *et al.* 1998). The advantage of the fractal description is that it eliminates the implied truncation at small length-scales, by assuming that the same power-law behaviour continues without limit as $\omega \to \infty$.

The qualitative nature of the contact process in this limit remains undetermined. In a recent paper, Borri-Brunetto *et al.* (1998) created a finite numerical realization of a surface with appropriate fractal properties and then used a numerical method to solve the resulting elastic contact problem at various levels of spatial discretization. With a coarse discretization, they obtained a few large actual contact areas, but as the grid was refined, these broke up progressively into clusters of smaller and smaller areas and the total area of actual contact decreased, following a characteristic power-law behaviour. This suggests that in the fractal limit the contact may consist of an infinite number of infinitesimal contact areas of total area zero. In other words, the actual contact area appears to be a fractal with dimension below two.

By contrast, Majumdar & Bhushan (1991) developed a theory of contact for fractal surfaces based on the 'bearing area' assumption (Johnson 1985, p. 407) that the distribution of actual contact area sizes would be similar to that of the 'islands' generated by cutting through the surface at a constant height z. Mandelbrot (1982) conjectures that the set of boundary curves obtained by this section has a fractal dimension one unit lower than the surface, but the set of islands themselves, which correspond to the assumed total contact area, clearly tends to a finite limit between zero and the extent of the nominal contact area.

The present paper seeks to investigate this issue by considering the elastic contact of a specialized two-dimensional fractal surface consisting of superposed sine waves of widely spaced wavelengths. We shall demonstrate that extended regions of contact are not possible with this model and we obtain results for the fractal dimension of the contact area by evaluating a sequence of truncated fractal series.

2. Westergaard's solution

We first consider the simple case of a two-dimensional elastic half-plane indented by a rigid body with a sinusoidal profile defined by the function

$$z(x) = g\cos(2\pi x/\lambda), \tag{2.1}$$

where g, λ are, respectively, the amplitude and wavelength of the sine wave.

If the mean pressure applied to the surface, $\bar{p} \geqslant p^*$, complete contact will be established and the contact pressure will be given by (Johnson 1985, § 13.2)

$$p(x) = \bar{p} + p^* \cos(2\pi x/\lambda), \tag{2.2}$$

where

$$p^* = \frac{\pi E g}{(1-\nu^2)\lambda} \tag{2.3}$$

and E, ν are Young's modulus and Poisson's ratio, respectively, for the material.

For $\bar{p} < p^*$, contact will be restricted to a series of regions at the peaks of the sine waves of width $2a$. A closed-form solution of this problem was given by Westergaard (1939). The contact pressure in a representative contact segment is given by

$$p(x) = \frac{2\bar{p}\cos(\pi x/\lambda)}{\sin^2(\pi a/\lambda)}\left[\sin^2\left(\frac{\pi a}{\lambda}\right) - \sin^2\left(\frac{\pi x}{\lambda}\right)\right]^{1/2}, \quad -a < x < a \tag{2.4}$$

and the half-length of the contact segment is

$$a = \frac{\lambda}{\pi}\arcsin\left(\frac{\bar{p}}{p^*}\right)^{1/2}. \tag{2.5}$$

If $\bar{p} \ll p^*$, these results reduce to the Hertzian values

$$p(x) = \frac{2\bar{p}\lambda}{\pi a}\sqrt{1 - \frac{x^2}{a^2}}, \tag{2.6}$$

$$a = \frac{\lambda}{\pi}\sqrt{\frac{\bar{p}}{p^*}}. \tag{2.7}$$

Figure 13.2 of Johnson (1985) shows that these results give an acceptable approximation to (2.4), (2.5) if

$$\bar{p}/p^* < 0.2. \tag{2.8}$$

We also record the maximum pressure at the peaks, $x = 0$, which is

$$p^{\max} = \bar{p} + p^*, \quad \bar{p} > p^*, \tag{2.9}$$

$$= 2\sqrt{\bar{p}p^*}, \quad 0 < \bar{p} < p^*, \tag{2.10}$$

from (2.4).

The cumulative pressure distribution function, $Q(p,\bar{p},p^*)$, can be defined as that proportion of the wavelength λ over which the contact pressure exceeds a given value, p. For full contact, $\bar{p} > p^*$,

$$Q(p,\bar{p},p^*) = 1, \quad p < \bar{p} - p^*, \tag{2.11}$$

$$= 0, \quad p > \bar{p} + p^*. \tag{2.12}$$

In the intermediate range, $\bar{p} - p^* < p < \bar{p} + p^*$, we note from equation (2.2) that the pressure will exceed p in the segment

$$-\frac{\lambda}{2\pi}\arccos\left(\frac{p-\bar{p}}{p^*}\right) < x < \frac{\lambda}{2\pi}\arccos\left(\frac{p-\bar{p}}{p^*}\right) \tag{2.13}$$

and hence

$$Q(p,\bar{p},p^*) = \frac{\lambda}{\pi}\arccos\left(\frac{p-\bar{p}}{p^*}\right), \quad \bar{p} - p^* < p < \bar{p} + p^*. \tag{2.14}$$

The probability distribution for contact pressure

$$q(p,\bar{p},p^*) = -\frac{\partial Q}{\partial p} = \frac{1}{\pi\sqrt{p^{*2} - (p-\bar{p})^2}}, \quad \bar{p} - p^* < p < \bar{p} + p^*, \tag{2.15}$$

$$= 0, \quad p < \bar{p} - p^* \text{ or } p > \bar{p} + p^* \tag{2.16}$$

is defined such that the probability of a given point having a pressure in the range $p, p + \delta p$ is $q(p)\delta p$.

Corresponding results for partial contact, $\bar{p} < p^*$, can be obtained in the same way by solving equation (2.4) for x to determine the length of the segment in which the pressure exceeds p. After some algebraic manipulations, we obtain

$$Q(p,\bar{p},p^*) = \frac{2}{\pi}\arcsin\sqrt{\frac{1}{2}\left\{\left(\frac{\bar{p}}{p^*}+1\right) - \sqrt{\left(1-\frac{\bar{p}}{p^*}\right)^2 + \left(\frac{p}{p^*}\right)^2}\right\}}, \quad 0 < p < 2\sqrt{p^*\bar{p}}, \tag{2.17}$$

$$= 0, \quad p > 2\sqrt{p^*\bar{p}} \tag{2.18}$$

and hence

$$q(p,\bar{p},p^*) = -\frac{\partial Q}{\partial p} = \frac{p}{\pi\sqrt{\{(p^*-\bar{p})^2 + p^2\}\{2\bar{p}(p^* - \bar{p} + \sqrt{(p^*-\bar{p})^2 + p^2}) - p^2\}}},$$

$$0 < p < 2\sqrt{p^*\bar{p}}, \tag{2.19}$$

$$= 0, \quad p > 2\sqrt{p^*\bar{p}}. \tag{2.20}$$

3. The Weierstrass function

Suppose now that instead of a single sine wave, the rough surface contains a series of superposed sinusoids, defined by the Weierstrass function (Weierstrass 1895; Berry & Lewis 1980)

$$z(x) = g_0 \sum_{n=0}^{\infty} \gamma^{(D-2)n} \cos(2\pi\gamma^n x/\lambda_0). \tag{3.1}$$

The amplitude and wavelength of the nth term are, respectively,

$$g_n = g_0\gamma^{(D-2)n}, \qquad \lambda_n = \lambda_0\gamma^{-n}, \tag{3.2}$$

where g_0, λ_0 are constants with dimensions of length and γ, D are dimensionless constants. If $\gamma > 1$ and $D > 1$, equation (3.1) defines a plane fractal surface of fractal† dimension D.

In contrast to the Weierstrass–Mandelbrot function (Berry & Lewis 1980), the function (3.1) has a largest scale and is bounded in the range

$$-\hat{z} < z(x) < \hat{z}, \tag{3.3}$$

where

$$\hat{z} = \frac{g_0}{1-\gamma^{(D-2)}}. \tag{3.4}$$

It satisfies the scaling relation

$$z(\gamma x) = \gamma^{2-D} z(x) - g_0\gamma^{2-D}\cos(2\pi x/\lambda_0) \tag{3.5}$$

and hence is self-affine except for an additive smooth function (Tél 1988). We also note that successive sinusoids in (3.1) satisfy the recurrence relations

$$g_{n-1}/g_n = \gamma^{2-D}, \qquad \lambda_{n-1}/\lambda_n = \gamma. \tag{3.6}$$

We first postulate that the mean pressure $\bar{p}$ is sufficient to cause full contact between the bodies. The elastic contact problem is then linear, since the inequality constraints precluding tensile tractions and negative gaps are inactive, and we can write down the corresponding pressure distribution by superposition of terms like equation (2.2) in the form

$$p(x) = \bar{p} + \sum_{n=0}^{\infty} p_n^* \cos(2\pi\gamma^n x/\lambda_0), \tag{3.7}$$

where

$$p_n^* = \frac{\pi E g_0 \gamma^{(D-1)n}}{(1-\nu^2)\lambda_0}. \tag{3.8}$$

This expression is bounded in the range

$$\bar{p} - \hat{p} \leqslant p(x) \leqslant \bar{p} + \hat{p}, \tag{3.9}$$

where

$$\hat{p} = \sum_{n=0}^{\infty} p_n^* \equiv \frac{\pi E g_0}{(1-\nu^2)\lambda_0} \sum_{n=0}^{\infty} \gamma^{(D-1)n}, \tag{3.10}$$

but for $\gamma > 1$, $D > 1$ the series in (3.10) does not converge, indicating that there is no finite value of mean pressure $\bar{p}$ that is sufficient to ensure complete contact between a fractal rigid surface of the form (3.1) and an elastic half-plane.

It is interesting to note that the series in equation (3.10) also diverges for the limiting case $D = 1$, showing that non-fractal surfaces can be defined for which complete elastic contact is unachievable.

† The fractal dimension of the Weierstrass function is discussed by Falconer (1990, § 11.1). For more general self-affine curves, see Mandelbrot (1985) and Borodich & Onishchenko (1999).

4. Partial contact

An ad hoc argument can be developed to show that there can be no contact segments of finite size even in the nonlinear problem with partial contact. Suppose that the contrary is true and that in the fractal limit there exists some contact segment A of finite length $2l$. We take a new origin at the midpoint of A and perform an asymptotic expansion of the solution in terms of the new variable $y = Mx$, where M is a suitably large number. In physical terms, this is equivalent to focusing attention on the immediate vicinity of the midpoint of A, using a powerful microscope. Terms in $p(x)$ associated with the low-order terms in $z(x)$ will appear as constants in this expansion and the endpoints ($x = \pm l$) of A will recede to $\pm\infty$. However, the fractal character of the surface ensures that we shall still see an infinite sequence of superposed sinusoids in the finite domain. The local influence of the inequality constraints outside A will therefore be vanishingly small and the argument of the preceding section shows that the local pressure distribution cannot be bounded as we add additional terms to the series. Thus at some value of n, the contact inequality $p > 0$ must be violated somewhere in the domain, contradicting the original hypothesis.

We therefore conclude that there will be no contact segments of finite size in the fractal limit and hence that the fractal dimension of the total contact area will be less than unity, as found by Borri-Brunetto *et al.* (1998). We shall explore these questions using a restricted form of the profile (3.1) in the next section.

5. Contact conditions near the asperity peaks

From this point on, we shall restrict attention to fractal surfaces of the form (3.1) in which $\gamma \gg 1$, so that there are many waves of scale n in one wavelength of scale $n-1$. Under these conditions, the pressure p_{n-1} at scale $n-1$ changes only slightly over one wavelength λ_n at scale n and hence the problem at scale n can be considered as a series of applications of Westergaard's solution in which the local value of p_{n-1} serves as the mean pressure $\bar{p}$. All the relations established in § 2 then carry over to this problem, with the substitutions

$$p \to p_n, \qquad \bar{p} \to p_{n-1}, \qquad p^* \to p_n^*. \tag{5.1}$$

As the ratio p_{n-1}/p_n^* increases, there will be a progression from 'Hertzian' contact, to partial contact described by the Westergaard equations (2.4), (2.5) and then to full contact. Now equation (3.8) shows that p_n^* increases with n, whereas the *average* value of p_{n-1} must remain constant at $\bar{p}$ from equilibrium considerations. We therefore anticipate that the contact process will become increasingly dominated by individual asperity contacts in the Hertzian regime with increasing n.

We can establish an upper bound on the value of p_{n-1}/p_n^* by considering the most heavily loaded asperities at any scale n, which are those near the peak of the pressure distribution at scale $n-1$. We denote this peak pressure by $p_{n-1}^{\max}$. It then follows from equations (2.9), (2.10) and (5.1) that

$$p_n^{\max} = p_n^* f(x_{n-1}), \tag{5.2}$$

where

$$x_{n-1} = p_{n-1}^{\max}/p_n^* \tag{5.3}$$

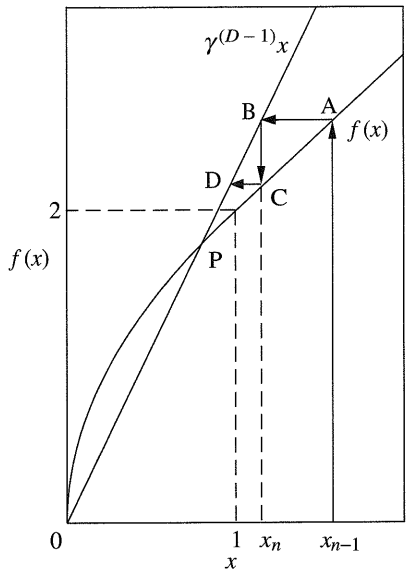

Figure 1. Graphical illustration of the iteration process defined by equation (5.6).

and

$$f(x) = 1 + x, \qquad x > 1, \tag{5.4}$$

$$= 2\sqrt{x}, \qquad 0 < x < 1. \tag{5.5}$$

We then have, using (3.8),

$$x_n \equiv \frac{p_n^{\max}}{p_{n+1}^*} = \frac{p_n^*}{p_{n+1}^*} f(x_{n-1}) = \gamma^{1-D} f(x_{n-1}). \tag{5.6}$$

Equation (5.6) defines an iteration of the form ABCD in figure 1 and it is readily verified that it converges monotonically on the unique positive non-zero solution of the equation

$$x = \gamma^{1-D} f(x) \tag{5.7}$$

for any positive starting value x_0. The solution of equation (5.7) corresponds to the point P in figure 1, where the straight line has slope γ^{D-1}. Substituting (5.4), (5.5) into (5.7) and solving for x_{P}, we obtain

$$x_{\mathrm{P}} = \frac{4}{\gamma^{2D-2}}, \qquad \gamma^{D-1} > 2, \tag{5.8}$$

$$= \frac{1}{(\gamma^{D-1} - 1)}, \qquad \gamma^{D-1} < 2, \tag{5.9}$$

corresponding to partial and full contact, respectively. We conclude that, for sufficiently large n, the maximum contact pressure

$$p_n^{\max} = p_n^* \gamma^{D-1} x_{\mathrm{P}}, \tag{5.10}$$

from (5.2), (5.7), where x_{P} is given by (5.8), (5.9).

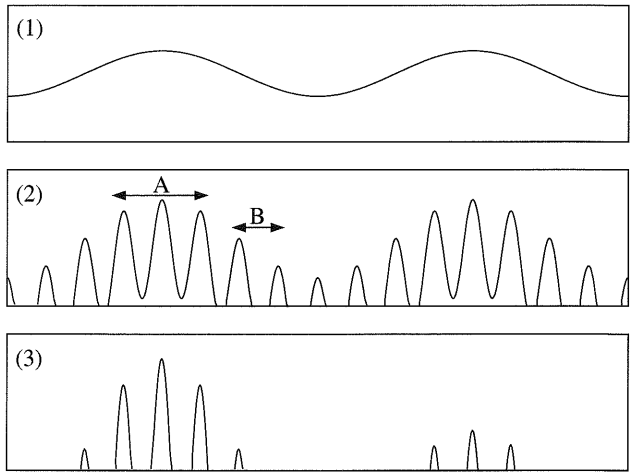

Figure 2. Evolution of the contact pressure distribution for $\gamma^{D-1} < 2$. A full contact region (1) evolves to (2) at the next scale. With one further reduction of scale, regions (2A) evolve once again to (2), while regions (2B) evolve to (3).

All asperities will be in the Hertzian regime at large n if the ratio $p_{n-1}^{\max}/p_n^* \to x_{\mathrm{P}}$ is sufficiently small. For example, the inequality (2.8) will be satisfied everywhere at large n as long as $x_{\mathrm{P}} < 0.2$ and hence

$$\gamma^{D-1} > \sqrt{20}, \tag{5.11}$$

from (5.8). In view of the monotonicity of the iteration of figure 1, (2.8) will be satisfied *at all scales* if in addition the largest scale sinusoid satisfies the condition

$$\tilde{p} \equiv \bar{p}/p_0^* < 0.2. \tag{5.12}$$

By a similar argument, there will be partial contact at every asperity for sufficiently large n if

$$\gamma^{D-1} > 2 \tag{5.13}$$

and for all n if in addition

$$\tilde{p} < 1. \tag{5.14}$$

The parameter range $\gamma^{D-1} < 2$ deserves some comment, since it predicts the existence of some regions of full contact at all scales and appears at first sight to contradict the argument of § 4. However, these regions become a vanishingly small proportion of the total number of asperity contacts as $n \to \infty$ and their sizes decrease at each scale. Figure 2 shows this process schematically for the case $\gamma^{D-1} < 2$. Each region of full contact (1) evolves into a smaller similar region (2A) at the next scale along with a region of separated contacts (2B). With one further reduction of scale, regions (2A) evolve once again to (2), while regions (2B) evolve to (3).

6. The contact pressure distribution

If we know the probability distribution function $q_{n-1}(p_{n-1})$ for contact pressure at scale $n-1$, we can determine the corresponding distribution at scale n by summing the contributions from the separate asperities. In view of (5.1), the function

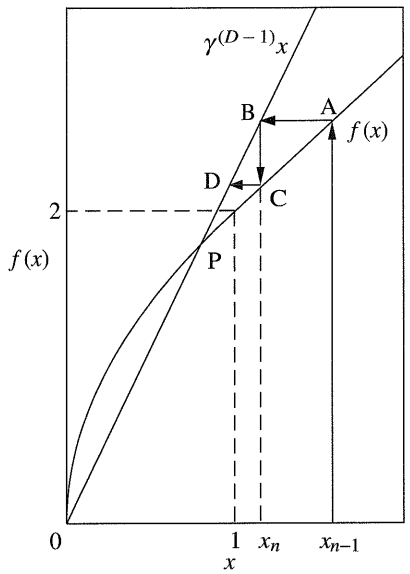

Figure 1. Graphical illustration of the iteration process defined by equation (5.6).

and

$$f(x) = 1 + x, \qquad x > 1, \tag{5.4}$$

$$= 2\sqrt{x}, \qquad 0 < x < 1. \tag{5.5}$$

We then have, using (3.8),

$$x_n \equiv \frac{p_n^{\max}}{p_{n+1}^*} = \frac{p_n^*}{p_{n+1}^*} f(x_{n-1}) = \gamma^{1-D} f(x_{n-1}). \tag{5.6}$$

Equation (5.6) defines an iteration of the form ABCD in figure 1 and it is readily verified that it converges monotonically on the unique positive non-zero solution of the equation

$$x = \gamma^{1-D} f(x) \tag{5.7}$$

for any positive starting value x_0. The solution of equation (5.7) corresponds to the point P in figure 1, where the straight line has slope γ^{D-1}. Substituting (5.4), (5.5) into (5.7) and solving for x_{P}, we obtain

$$x_{\mathrm{P}} = \frac{4}{\gamma^{2D-2}}, \qquad \gamma^{D-1} > 2, \tag{5.8}$$

$$= \frac{1}{(\gamma^{D-1} - 1)}, \qquad \gamma^{D-1} < 2, \tag{5.9}$$

corresponding to partial and full contact, respectively. We conclude that, for sufficiently large n, the maximum contact pressure

$$p_n^{\max} = p_n^* \gamma^{D-1} x_{\mathrm{P}}, \tag{5.10}$$

from (5.2), (5.7), where x_{P} is given by (5.8), (5.9).

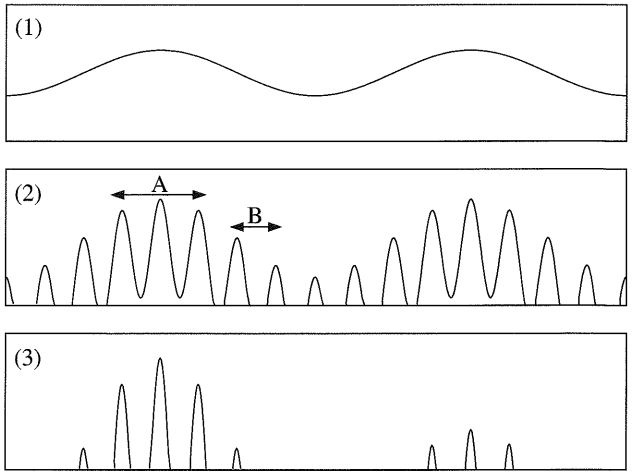

Figure 2. Evolution of the contact pressure distribution for $\gamma^{D-1} < 2$. A full contact region (1) evolves to (2) at the next scale. With one further reduction of scale, regions (2A) evolve once again to (2), while regions (2B) evolve to (3).

All asperities will be in the Hertzian regime at large n if the ratio $p_{n-1}^{\max}/p_n^* \to x_{\mathrm{P}}$ is sufficiently small. For example, the inequality (2.8) will be satisfied everywhere at large n as long as $x_{\mathrm{P}} < 0.2$ and hence

$$\gamma^{D-1} > \sqrt{20}, \tag{5.11}$$

from (5.8). In view of the monotonicity of the iteration of figure 1, (2.8) will be satisfied *at all scales* if in addition the largest scale sinusoid satisfies the condition

$$\tilde{p} \equiv \bar{p}/p_0^* < 0.2. \tag{5.12}$$

By a similar argument, there will be partial contact at every asperity for sufficiently large n if

$$\gamma^{D-1} > 2 \tag{5.13}$$

and for all n if in addition

$$\tilde{p} < 1. \tag{5.14}$$

The parameter range $\gamma^{D-1} < 2$ deserves some comment, since it predicts the existence of some regions of full contact at all scales and appears at first sight to contradict the argument of § 4. However, these regions become a vanishingly small proportion of the total number of asperity contacts as $n \to \infty$ and their sizes decrease at each scale. Figure 2 shows this process schematically for the case $\gamma^{D-1} < 2$. Each region of full contact (1) evolves into a smaller similar region (2A) at the next scale along with a region of separated contacts (2B). With one further reduction of scale, regions (2A) evolve once again to (2), while regions (2B) evolve to (3).

6. The contact pressure distribution

If we know the probability distribution function $q_{n-1}(p_{n-1})$ for contact pressure at scale $n-1$, we can determine the corresponding distribution at scale n by summing the contributions from the separate asperities. In view of (5.1), the function

$q(p_n, p_{n-1}, p_n^*)$ defined by equations (2.15), (2.16), (2.19) and (2.20) can be interpreted as the conditional probability of p_n, given p_{n-1}. Summation over all values of p_{n-1} then gives

$$q_n(p_n) = I_1 + I_2 \equiv \int_0^{p_n^*} q(p_n, p_{n-1}, p_n^*) q_{n-1}(p_{n-1})\,\mathrm{d}p_{n-1} + \int_{p_n^*}^{\infty} q(p_n, p_{n-1}, p_n^*) q_{n-1}(p_{n-1})\,\mathrm{d}p_{n-1}, \quad (6.1)$$

where we have split the integral into two ranges corresponding to partial contact (2.19), (2.20) and full contact (2.15), (2.16), respectively.

The inequalities in (2.15), (2.16), (2.19) and (2.20) impose further restrictions on the range of I_1, I_2, leading to the results

$$I_1 = \frac{1}{\pi} \int_{p_n^2/4p_n^*}^{p_n^*} \frac{q_{n-1}(p_{n-1}) p_n \,\mathrm{d}p_{n-1}}{\sqrt{\{(p_n^* - p_{n-1})^2 + p_n^2\}\{2p_{n-1}(p_n^* - p_{n-1} + \sqrt{(p_n^* - p_{n-1}) + p_n^2}) - p_n^2\}}}, \quad p_n < 2p_n^*, \quad (6.2)$$

$$= 0, \quad p_n > 2p_n^*, \quad (6.3)$$

$$I_2 = \frac{1}{\pi} \int_{p_n^*}^{p_n + p_n^*} \frac{q_{n-1}(p_{n-1})\,\mathrm{d}p_{n-1}}{\sqrt{p_n^{*2} - (p_n - p_{n-1})^2}}, \quad p_n < 2p_n^*, \quad (6.4)$$

$$= \frac{1}{\pi} \int_{p_n - p_n^*}^{p_n + p_n^*} \frac{q_{n-1}(p_{n-1})\,\mathrm{d}p_{n-1}}{\sqrt{p_n^{*2} - (p_n - p_{n-1})^2}}, \quad p_n > 2p_n^*. \quad (6.5)$$

For $n = 0$, we have $q_0(p_0) = q(p_0, \bar{p}, p_0^*)$ and hence equation (6.1) can be used recursively to determine $q_n(p_n)$ for any n.

(*a*) *Total contact area*

A similar argument can be used to determine the total contact area A_n at scale n in the segment λ_0, i.e. the sum of all the individual contact segments at scale n. We first note that the conditional probability of contact, given p_{n-1}, is unity for full contact ($p_{n-1} > p_n^*$) and is

$$\frac{2a}{\lambda} = \frac{2}{\pi} \arcsin\left(\frac{p_{n-1}}{p_n^*}\right)^{1/2} \quad (6.6)$$

for partial contact ($p_{n-1} < p_n^*$), from (2.5). It follows that the proportion of the segment L in contact at scale n is

$$\frac{A_n}{L} = \frac{2}{\pi} \int_0^{p_n^*} q_{n-1}(p_{n-1}) \arcsin\left(\frac{p_{n-1}}{p_n^*}\right)^{1/2} \mathrm{d}p_{n-1} + \int_{p_n^*}^{\infty} q_{n-1}(p_{n-1})\,\mathrm{d}p_{n-1}. \quad (6.7)$$

Numerical integration methods were used to determine $q_n(p_n)$ and hence A_n/λ_0 as functions of n for various values of γ, D and the dimensionless loading parameter

$$\tilde{p} = \bar{p}/p_0^*. \quad (6.8)$$

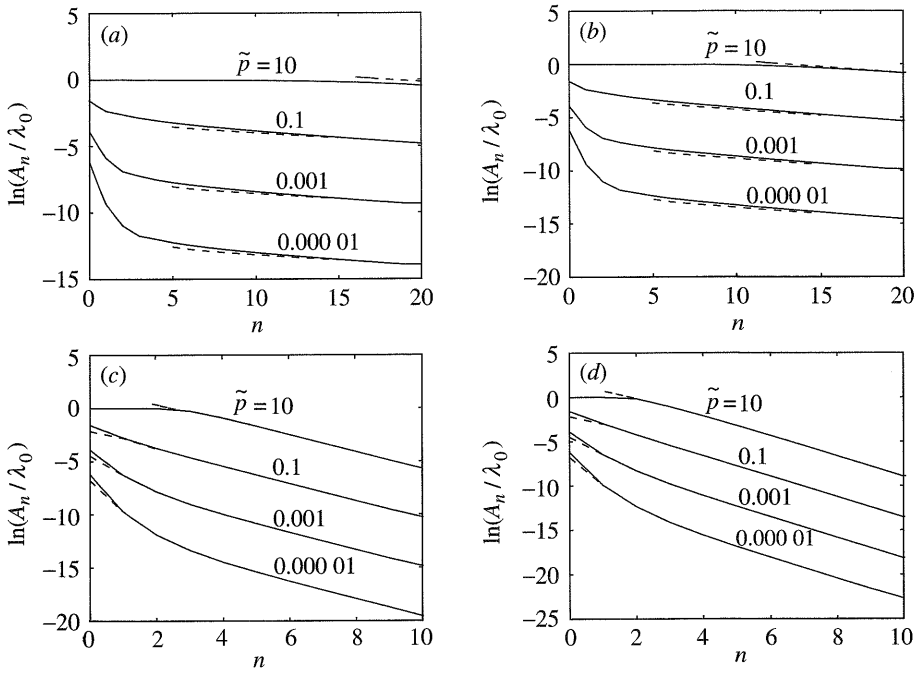

Figure 3. Variation of total contact area (A_n) with scale (n) for various values of $D, \gamma, \tilde{p}$, from equation (6.7). The dashed curves represent the Hertzian approximation developed in equation (7.18). (*a*) $D = 1.05$, $\gamma = 5$; (*b*) $D = 1.05$, $\gamma = 10$; (*c*) $D = 1.5$, $\gamma = 5$; (*d*) $D = 1.5$, $\gamma = 10$.

The contact area A_n/λ_0 is plotted logarithmically against n in figure 3. The most striking feature of these results is that at sufficiently large n they all tend to straight lines with a negative slope that depends upon D and γ, but not on $\tilde{p}$. If $\tilde{p} \geqslant 1$, the process starts in full contact ($A_0/\lambda_0 = 1$) and this may persist for several scales for large $\tilde{p}$. However, at larger n, the behaviour is increasingly dominated by partial and indeed Hertzian contact as predicted in § 5. For very light loads ($\tilde{p} \ll 1$), the opposite effect is observed, with the curves in figure 3 being initially steeper than the limiting slope. We conclude that the total contact area is not a simple fractal (in the sense that it deviates from the power-law form at low n), but this is hardly surprising in view of the nonlinearity inherent in the solution of the contact problem. However, the contact area does exhibit limiting power-law fractal behaviour at large n and in all cases the limiting slope is achieved at fairly modest values of n.

This conclusion requires some qualification when applied to the underlying physical contact problem, as distinct from the mathematical linear-elastic idealization. The higher-order terms in the Weierstrass series have increasingly high surface slopes and curvatures leading to increased contact pressure and the probability of plastic deformation or fracture. There must therefore be some n, depending on the value of the initial amplitude–wavelength ratio, g_0/λ_0, beyond which the idealization breaks down and qualitatively different results may be obtained. Of course, a similar restriction applies to any attempt to apply fractal arguments to a physical problem, since no part of the physical world exhibits refinement to smaller and smaller length-scales ad infinitum. The fractal mathematics can only be regarded as describing an asymp-

totic behaviour that holds until a sufficiently small scale is reached for the stated description to be unrealistic.

7. Archard's method

The results of figure 3 were obtained by successive numerical integration of equations (6.1), (6.7), but a closed-form expression for the limiting slope at large n can be obtained by extending the methodology of Archard (1957).

Archard (1957) considered a three-dimensional self-similar surface consisting of a single spherical asperity on which are superposed successive scales of smaller spherical asperities with uniform spatial distribution. An exactly parallel argument can be used for the two-dimensional Weierstrass profile of equation (2.1), whose peaks can be regarded as a self-affine sequence of uniformly distributed parabolas. The solution developed here uses the approximate Hertzian equations (2.6), (2.7), but this is not a serious restriction, since Hertzian contacts increasingly dominate the contact process at large n. Archard developed expressions for the total contact area as a function of force for the first three scales $n = 1, 2, 3$ and in each case obtained a power-law relation tending towards linearity as n increased. Here we generalize the procedure by establishing a recurrence relation between the expressions at scale n and $n + 1$ and hence reason inductively to an expression valid for all n.

For $\gamma \gg 1$, the pressure $p_n(x)$ at level n is approximately constant over one complete wave at level $n + 1$ and translates into a force

$$F_{n+1} = p_n(x)\lambda_{n+1} \tag{7.1}$$

on the corresponding asperity. The solution strategy is based on the fact that the sublevels $1 \leqslant m \leqslant n + 1$ can be mapped into $0 \leqslant m \leqslant n$. Thus, if we knew the total contact area A_n due to an applied force F_0, we could deduce the contribution to A_{n+1} associated with a single asperity at level 1 due to a given force F_1. Using equation (7.1) for F_1 and summation over the range of x would then give the value of A_{n+1}.

Archard's results for the sphere problem lead us to expect a power-law dependence of contact area on force at any scale, so we start by advancing the tentative hypothesis that

$$\frac{A_n}{\lambda_0} = K_n \gamma^{\alpha_n} \left(\frac{\lambda_0}{g_0}\right)^{\beta_n} \left(\frac{(1-\nu^2)F_0}{\pi E g_0}\right)^{\delta_n}, \tag{7.2}$$

where the groupings of parameters are dictated by dimensional considerations. In particular, we note that the dimensionless loading parameter

$$\frac{(1-\nu^2)F_0}{\pi E g_0} = \tilde{p} \tag{7.3}$$

using (2.3), (6.8), since $F_0 = \lambda_0 \bar{p}$.

The contact area for a single asperity at level 1 with n sublevels, loaded by a force F_1, is obtained by replacing g_0, λ_0, F_0 by g_1, λ_1, F_1, i.e.

$$\frac{A}{\lambda_1} = K_n \gamma^{\alpha_n} \left(\frac{\lambda_1}{g_1}\right)^{\beta_n} \left(\frac{(1-\nu^2)F_1}{\pi E g_1}\right)^{\delta_n}. \tag{7.4}$$

Using (7.1) for F_1 and (3.2) to write g_1, λ_1 in terms of g_0, λ_0, γ, we obtain

$$\frac{A}{\lambda_0} = K_n \gamma^{\rho} \left(\frac{\lambda_0}{g_0}\right)^{\beta_n} \left(\frac{(1-\nu^2)p_0(x)\lambda_0}{\pi E g_0}\right)^{\delta_n}, \tag{7.5}$$

where

$$\rho = \alpha_n - 1 + (1-D)(\beta_n + \delta_n). \tag{7.6}$$

Now A is the contribution to the total contact area A_{n+1} from a single asperity at level 1 and hence from a length $\lambda_1 = \lambda_0 \gamma^{-1}$ of the surface, so A_{n+1} can be found by integration as

$$\frac{A_{n+1}}{\lambda_0} = K_n \gamma^{\rho+1} \left(\frac{\lambda_0}{g_0}\right)^{\beta_n} \int_{-a_0}^{a_0} \left(\frac{(1-\nu^2)p_0(x)\lambda_0}{\pi E g_0}\right)^{\delta_n} \frac{\mathrm{d}x}{\lambda_0}. \tag{7.7}$$

Noting that $F_0 = \bar{p}\lambda_0$, we can rewrite the Hertzian relations (2.6), (2.7) in the form

$$p_0(x) = \frac{2F_0}{\pi a_0} \sqrt{1 - \frac{x^2}{a_0^2}}, \tag{7.8}$$

$$a_0 = \frac{\lambda_0}{\pi} \left(\frac{(1-\nu^2)F_0}{\pi E g_0}\right)^{1/2} = \frac{\lambda_0 \tilde{p}^{1/2}}{\pi} \tag{7.9}$$

and substitution into (7.7) yields

$$\frac{A_{n+1}}{\lambda_0} = 2^{\delta_n} K_n \gamma^{\rho+1} \pi^{(\delta_n - 3)/2} \left(\frac{\lambda_0}{g_0}\right)^{\beta_n} \tilde{p}^{(\delta_n+1)/2} \int_{-1}^{1} (1-\xi^2)^{\delta_n/2} \,\mathrm{d}\xi \tag{7.10}$$

$$\equiv K_{n+1} \gamma^{\alpha_{n+1}} \left(\frac{\lambda_0}{g_0}\right)^{\beta_{n+1}} \tilde{p}^{\delta_{n+1}}, \tag{7.11}$$

by analogy with (7.2).

We note that the result for A_{n+1} is of the same power-law form, thus justifying the initial choice in (7.2), and a comparison of the two expressions yields the recursive relations

$$\alpha_{n+1} = \alpha_n + (1-D)(\beta_n + \delta_n), \quad \beta_{n+1} = \beta_n, \quad \delta_{n+1} = \tfrac{1}{2}(\delta_n + 1) \tag{7.12}$$

and

$$\begin{aligned} K_{n+1} &= \frac{2^{\delta_n} K_n}{\pi} \int_{-1}^{1} (1-\xi^2)^{\delta_n/2} \,\mathrm{d}\xi \\ &= \frac{2^{\delta_n} K_n}{\sqrt{\pi}} \frac{\Gamma(1 + \frac{1}{2}\delta_n)}{\Gamma(\frac{3}{2} + \frac{1}{2}\delta_n)}, \end{aligned} \tag{7.13}$$

where $\Gamma(x)$ is the Euler Γ-function.

For $n = 0$, we have

$$\frac{A_0}{\lambda_0} = \frac{2a_0}{\lambda_0} = \frac{2}{\pi} \tilde{p}^{1/2}. \tag{7.14}$$

Table 1. *Values of* K_n

n	K_n	n	K_n	n	K_n	n	K_n	n	K_n
0	0.636 620	4	0.403 792	8	0.392 153	12	0.391 435	16	0.391 391
1	0.500 952	5	0.397 546	9	0.391 770	13	0.391 412	17	0.391 389
2	0.443 157	6	0.394 456	10	0.391 579	14	0.391 400	18	0.391 388
3	0.416 550	7	0.392 919	11	0.391 483	15	0.391 394	19	0.391 388

Thus,

$$\alpha_0 = 0, \quad \beta_0 = 0, \quad \delta_0 = \tfrac{1}{2}, \quad K_0 = 2/\pi \tag{7.15}$$

and it follows from (7.12), (7.13) that

$$\delta_n = 1 - 2^{-(n+1)}, \quad \beta_n = 0, \quad \alpha_n = (1-D)(n-1+2^{-n}), \tag{7.16}$$

$$K_n = \frac{2^{(n+2^{-n})}}{\pi^{(n+2)/2}} \prod_{i=0}^{n-1} \frac{\Gamma(1-2^{-(i+2)})}{\Gamma(\frac{3}{2}-2^{-(i+2)})}, \tag{7.17}$$

and

$$\frac{A_n}{\lambda_0} = \frac{2^{(n+2^{-n})}}{\pi^{(n+2)/2}} \prod_{i=0}^{n-1} \frac{\Gamma(1-2^{-(i+2)})}{\Gamma(\frac{3}{2}-2^{-(i+2)})} \gamma^{-(D-1)(n-1+2^{-n})} \tilde{p}^{(1-2^{-(n+1)})}. \tag{7.18}$$

Equation (7.18) is a closed-form expression defining the total extent of the contact area as a power-law function of $\bar{p}$ for any finite scale n. The two-dimensional (plane) equivalent of Archard's results for the first few scales can be obtained by substituting $n = 1, 2, 3$ into this equation.

Equation (7.16) shows that δ_n approaches unity as $n \to \infty$, confirming the trend noted by Archard (1957) that the nonlinear Hertzian relation between contact area and load approaches more closely to linearity as the number of superposed scales increases. However, the constant of proportionality gets smaller as n increases, principally through the influence of the term

$$\gamma^{\alpha_n} = \gamma^{-(D-1)(n-1+2^{-n})} \tag{7.19}$$

in equation (7.18). At large n, K_n tends to a limit, which can be evaluated as

$$K_\infty = \lim_{n\to\infty} K_n = 0.391\,39\ldots \tag{7.20}$$

and hence at large n,

$$A_n/\lambda_0 \approx K_\infty \gamma^{-(D-1)(n-1)} \tilde{p}. \tag{7.21}$$

In fact, K_n converges quite rapidly on the limit, the first 20 values being tabulated in table 1.

The expression (7.18) is plotted as a dashed line in figure 3. It is an extremely good approximation to the numerical results at large values of n—a result that is to be anticipated in view of the increasing prevalence of contacts in the Hertzian range at large n. More surprisingly, the Hertzian approximation performs very well even at the first few scales, except for the curves $\tilde{p} = 10$ in figure 3*a*, *b*.

We conclude that equation (7.21) defines the limiting behaviour of the system at large n and in particular that the limiting slope of the lines in figure 3 is

$$-(D-1)\ln(\gamma).$$

8. Characterization of the contact area

Following Tél (1988), we consider a partition of the interval λ_0 into γ^n subintervals each of length λ_n. If the origin in (3.1) is taken at the centre of λ_0, there will be a peak of the nth wave at the centre of each subinterval and it is clear from (7.1) that this peak will contribute a contact segment at level n if and only if $p_{n-1}(x) > 0$. This in turn requires that the point x be included in the contact area A_{n-1} at level $n-1$. The Hertzian approximation (7.18) then predicts that the number of contact segments in λ_0 at level n is

$$N(\lambda_0, \lambda_n) = A_{n-1}/\lambda_n = A_{n-1}\gamma^n/\lambda_0 \tag{8.1}$$

$$= K_{n-1}\gamma^{[(2-D)n+2(D-1)(1-2^{-n})]}\tilde{p}^{(1-2^{-n})}. \tag{8.2}$$

This expression defines a continuous (non-integer) function of γ which should be interpreted as the expected number of contact segments, since the contact area A_{n-1} will not generally be an integer multiple of λ_n. In the special case where the expected value of $N < 1$ it should be rounded up to unity, since physical considerations dictate a minimum of one contact segment in the domain λ_0. At large n, equation (8.2) approaches the value

$$N(\lambda_0, \lambda_n) \approx N_{\lim}(\lambda_0, \lambda_n) = K_\infty \gamma^{(2-D)n+2(D-1)}\tilde{p}. \tag{8.3}$$

Defining the dimensionless scale parameter (Tél 1988)

$$\epsilon = \lambda_n/\lambda_0 = \gamma^{-n}, \tag{8.4}$$

we have

$$n = -\frac{\ln(\epsilon)}{\ln(\gamma)} \tag{8.5}$$

and the limiting expression (8.3) can be written as

$$N_{\lim}(\lambda_0, \epsilon) = K_\infty \gamma^{2(D-1)}\epsilon^{-(2-D)}\tilde{p}, \tag{8.6}$$

showing that the limiting fractal dimension of the contact area is

$$d_{\mathrm{A}} = (2-D). \tag{8.7}$$

Equations (8.3), (7.21) show that, at any sufficiently fine resolution, both the total contact area and the number of contact areas are almost linear with the applied load, so that the average contact segment length is almost independent of load. This is consistent with the conclusions of classical theories of rough contact (see, for example, Greenwood & Williamson 1966).

Figure 4 shows a log–log plot of $N(\lambda_0, \epsilon)$ against ϵ for the cases considered in figure 3. The solid lines were obtained from equation (8.1) using the numerical results for A_{n-1} and hence apply over the complete range of contact conditions, while the

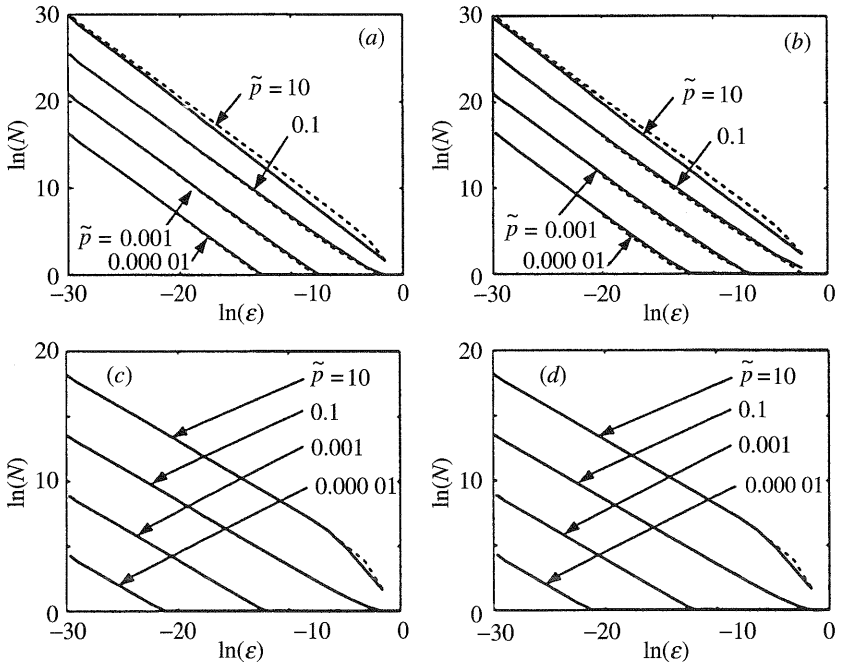

Figure 4. The number of contact areas (N) as a function of the dimensionless resolution ($\epsilon = \lambda_n/\lambda_0$) for various values of $D, \gamma, \tilde{p}$. The solid lines were obtained from equation (8.1) using the numerical results for A_{n-1} and the dotted lines represent the Hertzian approximation. (*a*) $D = 1.05$, $\gamma = 5$; (*b*) $D = 1.05$, $\gamma = 10$; (*c*) $D = 1.5$, $\gamma = 5$; (*d*) $D = 1.5$, $\gamma = 10$.

stippled line was obtained from the Hertzian approximation of equation (8.2). As in figure 3, the Hertzian approximation gives good results over almost all of the range of ϵ, except for large values of $\tilde{p}$. The results converge quite rapidly on the limiting expression (8.6) as ϵ decreases, but when ϵ approaches unity (low n) the deviation from the limiting form depends on the value of the loading parameter $\tilde{p}$. The results show that the 'apparent fractal dimension'—i.e. the slope of the line—increases significantly with $\tilde{p}$ at larger scales. Indeed, for sufficiently small values of $\tilde{p}$, several scales have to be passed before more than a single contact segment is predicted, corresponding to an apparent fractal dimension of zero.

This observation explains why Borri-Brunetto *et al.* (1998) reported a load dependence of fractal dimension in their numerical simulations. Computational limitations restricted their results to a maximum ratio of 2^8 between the smallest and largest scales and, in this region, the limiting fractal dimension was probably not fully established.

9. Distribution of contact segment lengths

The preceding analysis and results demonstrate clearly that, as we pass to smaller scales, the total contact area decreases and breaks into larger numbers of smaller segments. In this section, we determine the distribution of contact segment lengths at any given scale for cases that satisfy the conditions (5.13), (5.14) and hence do not involve any regions of full contact.

At any point where $p > p_{n-1}$, the individual contact segments developed at scale n must satisfy

$$a > \frac{\lambda_n}{\pi} \arcsin\left(\frac{p_{n-1}}{p_n^*}\right)^{1/2}, \tag{9.1}$$

since (2.5) defines a monotonic function of $\bar{p}$. The total number of contact segments per unit length with $a > a_n$ is therefore

$$N_n(a_n) = \frac{1}{\lambda_n} Q_{n-1}(p_{n-1}) = \frac{1}{\lambda_n} Q_{n-1}\left(p_n^* \sin^2\left(\frac{\pi a_n}{\lambda_n}\right)\right), \tag{9.2}$$

where $Q_{n-1}(p_{n-1})$ is the cumulative probability distribution corresponding to $q_{n-1}(p_{n-1})$, i.e. the probability that a given point will have a contact pressure $p > p_{n-1}$.

The total number of 'potential' contact segments per unit length is $1/\lambda_n$, so the normalized distribution function for a_n, i.e. the probability that a given asperity peak will lead to a contact segment with $a_n < a < a_n + \delta a_n$, is $\hat{N}_n(a_n)\delta a_n$, where

$$\hat{N}_n(a_n) = -\lambda_n N_n'(a_n) = \frac{\pi p_n^*}{\lambda_n} \sin\left(\frac{2\pi a_n}{\lambda_n}\right) q_{n-1}\left(p_n^* \sin^2\left(\frac{\pi a_n}{\lambda_n}\right)\right). \tag{9.3}$$

Figure 5 shows (a) the pressure distribution function $q_n(p_n)$ and (b) the distribution function for contact segment half-lengths $\hat{N}_n(a_n)$ for the case $D = 1.5$, $\gamma = 10$, $\tilde{p} = 0.001$. Both curves are presented in terms of normalized variables, $p_n/p_n^{\max}$, etc., since the range of pressures obtained increases rapidly (5.10) and the probability of contact at any given point decreases with reducing scale. Notice that $p_n^{\max}$ is given by equation (5.10) and $a_n^{\max}$ can be obtained by substituting this expression into (6.6), with the result

$$a_n^{\max} = \frac{\lambda_n}{\pi} \arcsin(x_{\mathrm{P}}), \tag{9.4}$$

where x_{P} is given by (5.8), (5.9).

Both distribution functions change character considerably during the first few scales, but they converge on a limiting normalized form as n increases, no significant deviation from this form being observed for $n > 20$. Similar behaviour was observed for other values of $D, \gamma, \tilde{p}$, but convergence was slower in cases that involved significant regions of contact outside the Hertzian range at low n. The converged normalized distributions depend upon the characteristics, D, γ, of the fractal surface, but are independent of the load $\tilde{p}$. Thus, the self-affine fractal character of the contact process at large n extends to the distributions of the contact parameters as well as to the integrated and averaged quantities.

10. Discussion

These results show that the contact process exhibits a limiting self-affine fractal behaviour at small scales, despite the nonlinearity of the elastic contact problem defined by Westergaard's solution (§ 2). In particular, the total contact area is a lacunar fractal, as predicted from the numerical simulation of Borri-Brunetto *et al.* (1998) and in contrast to the predictions of Majumdar & Bhushan (1995). Other features

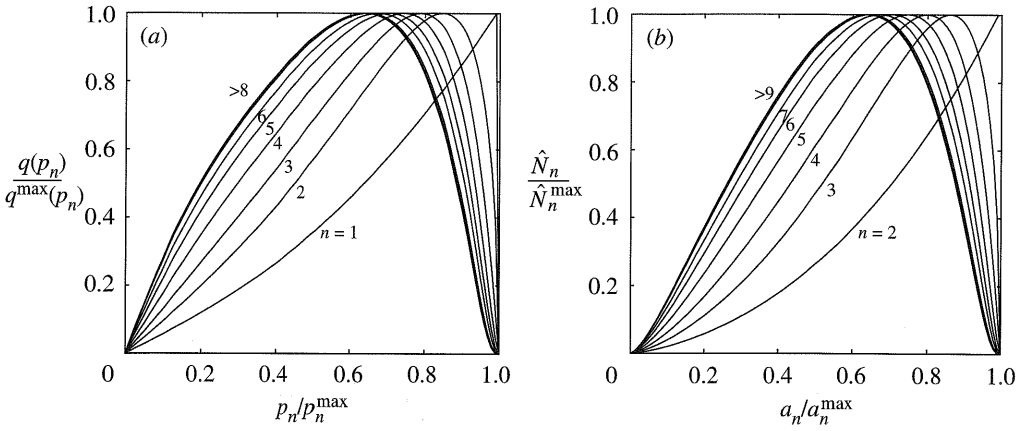

Figure 5. Evolution of the normalized distribution functions for (*a*) contact pressure and (*b*) contact segment length with the scaling parameter, n.

of Borri-Brunetto *et al.*'s simulation are also elucidated by the present analysis—notably their observation that the fractal dimension of the contact area increases with the applied load. Figure 4 shows that this is precisely the behaviour to be expected from the *apparent* fractal dimension—i.e. the slope of the $N - \epsilon$ curve—at relatively coarse scales, but that at smaller ϵ the fractal behaviour should become independent of load.

In making this comparison, it is important to recognize that the simulation of Borri-Brunetto *et al.* (1998) describes a three-dimensional contact problem, whereas the present analysis is two dimensional. Thus, their nominal contact region is an area (dimension 2), while ours is a line segment (of length λ_0 and dimension 1). An equivalent three-dimensional problem can be defined from equation (3.1) by assuming that the profile is independent of the orthogonal Cartesian coordinate y, in which case the line segments defining individual asperity contacts would represent contact strips. With this interpretation, both the fractal dimension of the surface D and that of the total contact area $2 - D$ would need to be incremented by unity, suggesting a limiting fractal dimension of $4-D$ to compare with Borri-Brunetto *et al.*'s simulation. All the results they report fall short of this limit. For example, with a surface of dimension 2.5, they obtained a maximum apparent fractal dimension (at high load) of 1.2, where our predicted limit would be 1.5. However, most practical surfaces are sufficiently rough even on the coarsest scales to place the individual asperity contacts firmly in the Hertzian range (Johnson 1985, § 13.1), implying that $\tilde{p} \ll 1$. In this range, figure 4 leads us to expect an apparent fractal dimension lower than the limiting value, as observed by Borri-Brunetto *et al.* (1998).

The present analysis is clearly extremely idealized, both because of the restriction to $\gamma \gg 1$ (required to permit the decoupling of scales) and to linear elastic behaviour, which must cause the model to become inappropriate at sufficiently large n. However, there is every reason to believe that qualitatively similar behaviour would be obtained at more realistic values of γ, as indeed is confirmed by the above comparison with the results of Borri-Brunetto *et al.* (1998).

The fractal description of any physical phenomenon must become inappropriate at sufficiently small scale and the utility of the description in any practical application

depends upon whether the essential physics of interest is adequately characterized within the range of applicability. In the present case, plastic deformation or fracture is likely to modify the behaviour at sufficiently large n, but an additional question is whether the important physical effects are largely determined by the limiting fractal behaviour at large n, or by the first few scales, where the apparent fractal dimension varies with load. However, regardless of the answer to these questions, it is generally desirable to use a surface characterization that does not contain an arbitrary (measurement precision determined) truncation limit.

11. Conclusions

These results show that for a plane surface defined by the Weierstrass series with admittedly rather restricted values of the scaling parameter γ, the contact area shows fractal characteristics with a limiting fractal dimension at large n of $(2 - D)$, where D is the fractal dimension of the surface. The results confirm the conclusion reached numerically by Borri-Brunetto *et al.* (1998) that the contact area is defined by a fractal set, i.e. that contact is restricted to an infinite set of infinitesimal contact segments in the limit $n \to \infty$; there are no contact segments of finite dimension and the total contact area tends regularly to zero. In addition, the deviation from simple power-law fractal behaviour at low wavenumbers provides an explanation of their observation that the apparent fractal dimension is load dependent. Even at large n, the splitting of segments of the contact area does not follow a 'simple' rule for successive scales. Without recourse to advanced multiscale multifractal analysis (Carpinteri & Chiaia 1997), we use a recursive formulation to obtain the distribution functions, indicating their dependence on geometrical characteristics of the profile.

J.R.B. is pleased to acknowledge support from the National Science Foundation under contract number CMS-9619527.

References

Archard, J. F. 1957 Elastic deformation and the laws of friction. *Proc. R. Soc. Lond.* A **243**, 190–205.

Berry, M. V. & Lewis, Z. V. 1980 On the Weierstrass–Mandelbrot fractal function. *Proc. R. Soc. Lond.* A **370**, 459–484.

Borodich, F. M. & Mosolov, A. B. 1992 Fractal roughness in contact problems. *J. Appl. Math. Mech.* **56**, 681–690.

Borodich, F. M. & Onishchenko, D. A. 1999 Similarity and fractality in the modelling of roughness by a multilevel profile with hierarchical structure. *Int. J. Solids Struct.* **36**, 2585–2612.

Borri-Brunetto, M., Carpinteri, A. & Chiaia, B. 1998 Lacunarity of the contact domain between elastic bodies with rough boundaries. In *Probamat-21st century: probabilities and materials* (ed. G. Frantziskonis), pp. 45–64. Dordrecht: Kluwer.

Carpinteri, A. & Chiaia, B. 1997 Multifractal scaling laws in the breaking behavior of disordered materials. *Chaos, Solitons Fractals* **8**, 135–150.

Falconer, K 1990 *Fractal geometry.* Wiley.

Greenwood, J. A. 1984 A unified theory of surface roughness. *Proc. R. Soc. Lond.* A **393**, 133–157.

Greenwood, J. A. & Williamson, J. B. P. 1966 The contact of nominally flat surfaces. *Proc. R. Soc. Lond.* A **295**, 300–319.

Johnson, K. L. 1985 *Contact mechanics.* Cambridge University Press.

Lopez, J., Hansali, G., Le Bossé, J. C. & Mathia, T. 1994 Caracterisation fractale de la rugosité tridimensionelle d'une surface. *J. Physique* **4**, 2501–2219.

Majumdar, A. & Bhushan, B. 1990 Role of fractal geometry in roughness characterization and contact mechanics of surfaces. *ASME Jl Tribol.* **112**, 205–216.

Majumdar, A. & Bhushan, B. 1991 Fractal model of elastic–plastic contact between rough surfaces. *ASME Jl Tribol.* **113**, 1–11.

Majumdar, A. & Bhushan, B. 1995 Characterization and modeling of surface roughness and contact mechanics. *Handbook of micro/nano tribology.* pp. 109–165. New York: Chemical Rubber Company.

Mandelbrot, B. B. 1982 *The fractal geometry of nature* San Francisco: Freeman.

Mandelbrot, B. B. 1985 Self affine fractals and fractal dimension. *Physica Scr.* **32**, 37–60.

Nayak, P. R. 1971 Random process model of rough surfaces. *ASME Jl Lubrication Technol.* **93**, 398–407.

Russ, J. C. 1994 *Fractal surfaces.* New York: Plenum.

Tél, T. 1988 Fractals, multifractals, and thermodynamics: an introductory review. *Z. Naturf.* A **43**, 1154–1174.

Weierstrass, K. 1895 *Mathematische werke.* Berlin: Mayer and Muller.

Westergaard, H. M. 1939 Bearing pressures and cracks. *ASME Jl Appl. Mech.* **6**, 49–53.

Whitehouse, D. J. & Phillips, M. J. 1978 Discrete properties of random surfaces. *Phil. Trans. R. Soc. Lond.* A **290**, 267–298.

Whitehouse, D. J. & Phillips, M. J. 1982 Two-dimensional discrete properties of random surfaces. *Phil. Trans. R. Soc. Lond.* A **305**, 441–468.